COMPUTATION OF FIELDS AND FORCES IN MAGNETIC FORCE MICROSCOPY

M. Mansuripur
Optical Sciences Center, University of Arizona, Tucson, Arizona 85721

Abstract

A model for the magnetization of the needle and its interaction with the sample in magnetic force microscopy is described. The model takes full account of the micromagnetic interactions involved.

Introduction

Magnetic force microscopy (MFM)[1] is an offshoot of scanning tunneling microscopy (STM)[2] and has the potential for high-resolution (~100 Å) observations of magnetic domains and domain walls. In MFM a sharp magnetic needle interacts with the field pattern established by the sample near its surface. A cantilever then converts the force on the needle to a displacement, which is measured interferometrically or otherwise.[3] In this paper we describe a model for the tip that takes full account of the micromagnetic interactions involved. An example of the force computation is also presented.

A Model for the Magnetization of the Needle

The needle's model used in this paper is shown in Figure 1. The tip and the stem are treated separately as indicated. The cubes that comprise the needle's tip are arranged in layers parallel to the XY plane. Thus the needle's axis is along Z and the centers of the cubes in the kth layer are at z_k where

$$z_k = z_1 + (k - 1)\Delta . \quad (1)$$

Here z_1 is the vertical coordinate of the center of the cube at the sharp end of the needle, and Δ is the linear dimension of the cubes. Within each layer the cubes are arranged in a square, centered on the needle's axis. The number of cubes in layer k will be denoted N_k^2. Although no restrictions are imposed on the values of Δ and N_k, in practice Δ should correspond to the average grain (crystallite) size of the needle's material and N_k's must be chosen in accordance with the geometry of the tip. Figure 2 shows cross sections of the tip for two sets of values of N_k. In (*a*) $N_1 = 1$, $N_2 = 2$, $N_3 = 3$, $N_4 = N_5 = N_6 = 4$, for a total of 62 cubes and a cone angle of $\Theta \simeq 53^0$. In (*b*) $N_1 = N_2 = 1$, $N_3 = N_4 = 2$, $N_5 = N_6 = 3$, $N_7 = N_8 = N_9 = N_{10} = 4$, for a total of 92 cubes and a cone angle of $\Theta \simeq 28^0$.

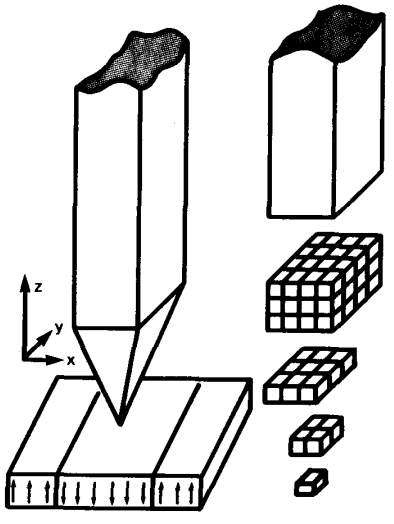

Fig.1 Magnetic needle scanning the surface of a magnetic film. The micromagnetic model treats the tip as a collection of cubical elements.

Each cube corresponds to a crystallite in the actual needle; therefore, a single dipole of strength μ is assigned to each cube. Assuming that the needle's material has saturation magnetization M_s, the assigned dipole moment's strength will be

$$\mu = M_s \Delta^3 . \quad (2)$$

The orientation of these moments in space is not arbitrary and depends on a number of factors that will be identified in the remainder of this section. To begin with, each grain has one or more easy axes depending on its crystalline structure and shape. For the sake of simplicity, we shall assume that each dipole has uniaxial anisotropy[4] of strength K_u. Both K_u and the direction of the easy axis for individual lattice sites are parameters that can be arbitrarily assigned.

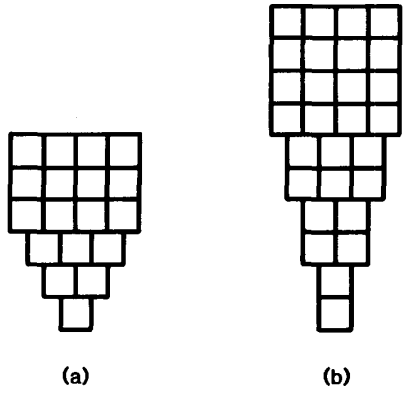

Fig.2 Two possible cross sections of the tip.

The second factor that plays a role in determining the magnetization of the needle is exchange interaction between neighboring grains at their common boundaries.[4] This interaction is represented by an equivalent exchange field that tends to align a given dipole with its nearest neighbor. The exchange field between a pair of cubes in full contact is denoted by H_{xhg}; when only a fraction of the adjacent surfaces of the two cubes make contact, the exchange field is proportionally reduced. Since direct methods for the measurement of the exchange field do not presently exist, H_{xhg} shall be treated as an adjustable parameter.

Classical dipole-dipole interactions make a significant contribution to the forces that determine the state of magnetization of the needle. The dipolar field is long-range and must be computed between each and every pair of dipoles. The fact that cubes of uniform magnetization are replaced by point dipoles is the source of some inaccuracy in the calculation of dipole-dipole (demagnetizing) interactions. Nonetheless, given the nature of the model and the degree of approximation brought about by our other assumptions, the errors involved in demagnetization calculations are quite acceptable.

Finally, the tip's magnetization is influenced by the magnetic charges in the stem and by the external field produced by sources outside the needle (such as the magnetic surface being probed by the tip). The effect of the external field will be treated in the next section. As for the stem, one possibility is to assume that it is magnetically hard and saturated along the Z axis. The exchange field acting on the lattice sites just below the stem will then be $H_{xhg}\hat{z}$. Calculation of the demagnetizing field of the stem on individual dipoles of the tip, arising from the uniform charge distribution on the stem's bottom surface, is rather straightforward.

0018-9464/89/0900-3467$01.00©1989 IEEE

Computation of the Stray Magnetic Field for a Thin Film

Consider a magnetic film of thickness h in the XY plane. The film's magnetization is uniform through the thickness and is therefore represented by $\mathbf{M}(x, y)$. The magnetic field $\mathbf{H}(x, y, z)$ and the gradients of the field components can be computed with the aid of Fourier transforms.[5] Since details of the Fourier technique have already been published this discussion shall focus only on the main points. The region of the XY plane used in field computations has dimension $L_x \times L_y$. Due to the periodic nature of the Fourier series, however, it is as though the entire XY plane were covered with identical tiles of dimension $L_x \times L_y \times h$. (Artificial effects of this periodic boundary condition remain confined to the region near the boundary.) The Fourier components of $\mathbf{M}(x, y)$ are

$$\mathbf{M}_{mn} = \frac{1}{L_x L_y} \int_0^{L_x} \int_0^{L_y} \mathbf{M}(x,y) \exp\left[-i2\pi\left(\frac{mx}{L_x} + \frac{ny}{L_y}\right)\right] \mathrm{dxdy} . \quad (3)$$

In the frequency domain f only discrete frequencies with $f_x = m/L_x$ and $f_y = n/L_y$ are allowed. The magnitude of the vector f is

$$f = |\mathbf{f}| = \sqrt{f_x^2 + f_y^2} = \sqrt{(m/L_x)^2 + (n/L_y)^2} . \quad (4)$$

Now consider the magnetic field $\mathbf{H}(x, y)$ in a plane $Z = z$ above the film's surface. (Since the film's midplane is at $Z = 0$ the results apply only to the region $z \geq h/2$.) Periodicity of $\mathbf{M}(x, y)$ implies that $\mathbf{H}(x, y)$ in the plane $Z = z$ is also periodic, therefore,

$$\mathbf{H}(x, y, z) = \sum_{m=-\infty}^{\infty} \sum_{n=-\infty}^{\infty} \mathbf{H}_{mn}(z) \exp\left[i2\pi\left(\frac{mx}{L_x} + \frac{ny}{L_y}\right)\right] . \quad (5)$$

The Fourier component $\mathbf{H}_{mn}$ of the field depends only on the Fourier component of the magnetization with the same frequency. The relationship between $\mathbf{H}_{mn}$ and $\mathbf{M}_{mn}$ is [5]

$$\mathbf{H}_{mn}(z) = -4\pi \exp(-2\pi f z) \sinh(\pi h f) (\mathbf{M}_{mn} \cdot \sigma_{mn}) \sigma_{mn} . \quad (6)$$

In Eq. (6) f is the magnitude of the frequency vector $\mathbf{f}$ as given by Eq. (4), and the complex vector σ_{mn} is defined as

$$\sigma_{mn} = \frac{f_x}{f} \hat{x} + \frac{f_y}{f} \hat{y} + i \hat{z} . \quad (7)$$

Note that the explicit dependence of the field on film thickness h can be removed by normalizing L_x, L_y, x, y and z by h. Also notice that Eqs. (3), (5), and (6) imply that the field distribution at $Z = z$ is merely a filtered version of the magnetization pattern $\mathbf{M}(x, y)$. The Fourier transforms in Eq. (3) and Eq. (5) are computed with a two-dimensional FFT algorithm.

The average magnetic field over the volume of a cube could be obtained with only a small additional effort. Consider a cube of dimension Δ, centered at (x_0, y_0, z_0), with sides parallel to the X, Y, Z axes. The average field

$$\mathbf{H}_{ave}(x_0, y_0, z_0) = \frac{1}{\Delta^3} \int_{z_0 - \frac{\Delta}{2}}^{z_0 + \frac{\Delta}{2}} \int_{y_0 - \frac{\Delta}{2}}^{y_0 + \frac{\Delta}{2}} \int_{x_0 - \frac{\Delta}{2}}^{x_0 + \frac{\Delta}{2}} \mathbf{H}(x,y,z) \, \mathrm{dxdydz}$$

can be determined from Eqs. (3), (5), (6) provided that the right side of Eq. (6) is multiplied by the (frequency-dependent) constant C_{mn}:

$$C_{mn} = \frac{\sin(\pi \Delta f_x)}{\pi \Delta f_x} \cdot \frac{\sin(\pi \Delta f_y)}{\pi \Delta f_y} \cdot \frac{\sinh(\pi \Delta f)}{\pi \Delta f} . \quad (8)$$

In other words, the average field computation requires only the modification of the spatial filter described in Eq. (6).

Micromagnetics of the Needle

Each grain (crystallite) of magnetic matter within the needle is subject to magnetic forces of various origins. Local anisotropy, exchange interaction with nearest neighbors, demagnetizing field produced by all the other grains in the needle, and the externally applied field add up to create a single effective magnetic field $\mathbf{H}^{(eff)}$ acting on each grain. Now if the grain's dipole moment is denoted by $\boldsymbol{\mu}$, the Landau-Lifshitz-Gilbert equation[6] describes the dynamics of this dipole's gyration as follows :

$$\dot{\boldsymbol{\mu}} = \gamma \boldsymbol{\mu} \times \left(\mathbf{H}^{(eff)} + \frac{\alpha \dot{\boldsymbol{\mu}}}{\gamma |\boldsymbol{\mu}|}\right) . \quad (9)$$

In this equation $\dot{\boldsymbol{\mu}}$ is the time derivative of $\boldsymbol{\mu}$, γ is the gyromagnetic ratio, and α is the viscous damping coefficient.

To determine a stable configuration for the tip magnetization, the starting point is to assign an initial direction to each dipole in the lattice. The effective field $\mathbf{H}^{(eff)}$ is then computed for each site and the system of dipoles is relaxed in accordance with the Landau-Lifshitz-Gilbert equation. The procedure is repeated until a stable configuration (i.e., local minimum of energy) is obtained. Details of the simulation algorithm can be found in Ref. 7.

Once the state of magnetization is determined, the net force on the needle is computed by adding the force of the external field experienced by individual grains. The force on a point dipole $\boldsymbol{\mu}$ in the field $\mathbf{H}(x, y, z)$ is

$$\mathbf{F} = \nabla [\boldsymbol{\mu} \cdot \mathbf{H}(x, y, z)] . \quad (10)$$

In matrix notation Eq. (10) is written

$$\begin{bmatrix} F_x \\ F_y \\ F_z \end{bmatrix} = \begin{bmatrix} \partial H_x/\partial x & \partial H_y/\partial x & \partial H_z/\partial x \\ \partial H_x/\partial y & \partial H_y/\partial y & \partial H_z/\partial y \\ \partial H_x/\partial z & \partial H_y/\partial z & \partial H_z/\partial z \end{bmatrix} \begin{bmatrix} \mu_x \\ \mu_y \\ \mu_z \end{bmatrix} . \quad (11)$$

Since $\nabla \times \mathbf{H} = 0$ the 3×3 matrix of gradients in Eq. (11) must be symmetric (i.e., $\partial H_y/\partial x = \partial H_x/\partial y$ and so on); therefore only six out of the nine elements of this matrix need to be evaluated.

Using Eqs. (5) and (6), one can derive the Fourier series representation for each row of the gradient matrix as follows :

$$\frac{\partial \mathbf{H}}{\partial x} = \sum_{m=-\infty}^{\infty} \sum_{n=-\infty}^{\infty} i2\pi f_x \mathbf{H}_{mn}(z) \exp\left[i2\pi\left(\frac{mx}{L_x} + \frac{ny}{L_y}\right)\right] \quad (12a)$$

$$\frac{\partial \mathbf{H}}{\partial y} = \sum_{m=-\infty}^{\infty} \sum_{n=-\infty}^{\infty} i2\pi f_y \mathbf{H}_{mn}(z) \exp\left[i2\pi\left(\frac{mx}{L_x} + \frac{ny}{L_y}\right)\right] \quad (12b)$$

$$\frac{\partial \mathbf{H}}{\partial z} = \sum_{m=-\infty}^{\infty} \sum_{n=-\infty}^{\infty} (-2\pi f) \mathbf{H}_{mn}(z) \exp\left[i2\pi\left(\frac{mx}{L_x} + \frac{ny}{L_y}\right)\right] . \quad (12c)$$

The force components in Eq. (11) must be averaged over the volume of the cube corresponding to the dipole $\boldsymbol{\mu}$. Since $\boldsymbol{\mu}$ is constant throughout the cube the averaging is done over the field gradients. The procedure is similar to the one described in the previous section regarding the averaging of $\mathbf{H}$, and so is the result : The average field gradients are still obtained from Eqs. (12) provided that the $\mathbf{H}_{mn}(z)$ of Eq. (6) are first multiplied by the C_{mn} of Eq. (8).

Finally, the force experienced by the tip must be added to the force exerted on the stem. For a hard stem saturated along Z this force is obtained by a simple integration of the external field over the charges on the bottom surface.

Results and Discussion

Consider a needle with the tip cross section as shown in Fig. 2(*a*). Let M_s = 1500 emu/cm^3, K_u = 10^7 erg/cm^3, H_{xhg} = 1000 *Oe*, and the axes of anisotropy have random directions in space. Other parameters of the model are Δ = 250 Å, α = 0.5, and γ = -10^7 Oe^{-1}. sec^{-1}. We started the simulation with all dipoles aligned in the +*Z* direction and relaxed the interacting system of dipoles following the Landau-Lifshitz-Gilbert equation. The energy of the system was computed during the relaxation process and is shown in Figure 3. It is observed that the contributions of both anisotropy and demagnetization to the total energy decrease in the process, while the contribution of exchange increases. The total energy is a decreasing function of time, as expected.

After about 500 iterations (corresponding to 300 psec. in Fig. 3) the magnetization of the tip reached a stable configuration which is shown in Fig. 4. By this time the average magnetization along *Z* has dropped from M_s = 1500 emu/cm^3 to $\langle M_z \rangle$ = 886 emu/cm^3.

Next we calculate the field and field gradients for a film with thickness h = 300 Å and saturation magnetization M_{so} = 100 emu/cm^3. The film is magnetized perpendicular to its surface and contains two straight domain walls, both parallel to the *Y* axis. The center of the first wall is at X = 800 Å while that of the second wall is at X = 2400 Å. The basic pattern of magnetization is defined between X = 0 and $X = L_x$ = 3200 Å. The wall thickness parameter δ_w is 75 Å and the wall structure is a simple Bloch wall with $\Theta(x)$ and $\phi(x)$ given by [6,7]

$$\tan\left[\frac{\Theta(x)}{2}\right] = \exp\left[\frac{x-x_0}{\delta_w}\right] \qquad (13a)$$

$$\phi(x) = \frac{\pi}{2} \qquad (13b)$$

The field and field gradients are computed with an FFT algorithm, using a sampling interval of 25 Å .

When the needle is brought to the film's vicinity, the tip's dipoles are allowed to relax further in order to conform to the field of the magnetic film. For the particular set of parameters used in these calculations, we found that the effect on the magnetization of the tip was small : depending on the position of the needle along *X*, the average *Z* component, $\langle M_z \rangle$, varied within ±1% of its value at zero field. With the needle's magnetization in a stable state, we calculated the force and then repeated the procedure for the next point along X. Figure 5 shows F_x and F_z as functions of x in the interval $0 \le x \le 1600$ Å. (The wall is at the midpoint of this interval.) The separation between the sharp end of the tip and the sample is 100 Å. Note that the peak of F_x and the zero-crossing of F_z occur at the wall center.

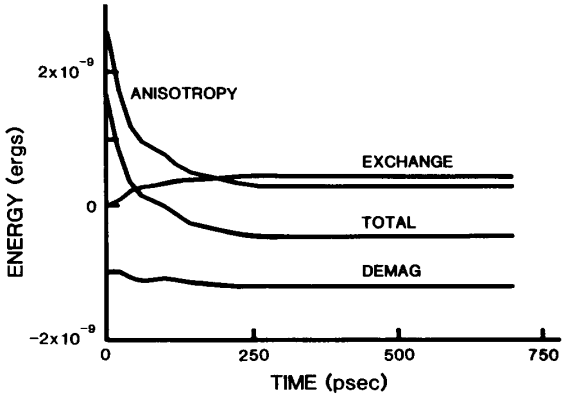

Fig.3 Various magnetic energies of the needle during the relaxation process. At t = 0 the dipoles are along the *Z* axis but by t = 300 psec. they have settled into a locally stable configuration.

Fig.4 Magnetization of the tip in the steady state. The state of each dipole is shown by an arrow with an appendage. The arrow is the component of magnetization along *Z* while the appendage is its component in the XY plane. Different blocks of arrows in this figure correspond to different layers of cubes in the tip's model shown in Figure 1.

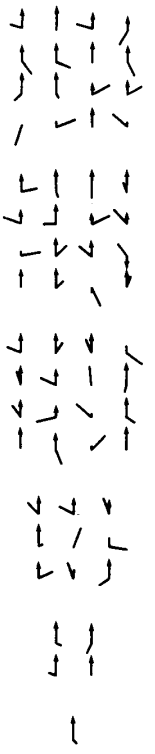

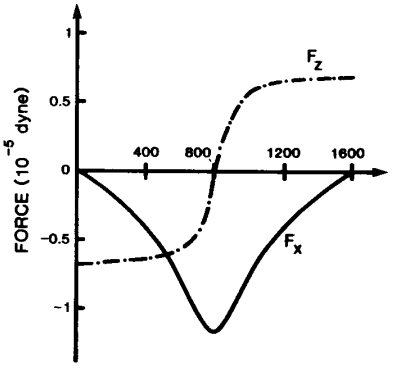

Fig.5 Horizontal and vertical components of force versus tip's position along X. The sample has perpendicular magnetization with a straight Bloch wall at x = 800 Å.

Acknowledgment

This work has been supported by the Optical Data Storage Center at the University of Arizona and by a grant from the IBM Corporation.

References

[1] Y. Martin, D. Rugar, and H. Wickramasinghe, "High-resolution magnetic imaging of domains in TbFe by force microscopy," *Appl. Phys. Lett.*, **vol. 52**, *p.* 244 (1988).

[2] G. Binnig, H. Rohrer, C. Gerber, and E. Weibel, "Tunneling through a controllable vacuum gap," *Appl. Phys. Lett.*, **vol. 40**, *p.* 179 (1982).

[3] D. Rugar, H. Mamin, R. Erlandsson, J. Stern, and B. Terris, "Force microscope using a fiber-optic displacement sensor," *Rev. Sci. Instr.*, **vol. 59**, *pp.* 2337-2340 (1988).

[4] A. H. Morrish, *The Physical Principles of Magnetism*, Wiley, New York, 1965.

[5] M. Mansuripur and R. Giles, "Demagnetizing field computation for dynamic simulation of the magnetization reversal process," *IEEE Trans. Mag.*, **vol. 24**, *pp.* 2326-2328 (1988).

[6] A. P. Malozemoff and J. C. Slonczewski, *Magnetic Domain Walls in Bubble Materials*, Academic Press, New York, 1979.

[7] M. Mansuripur, "Magnetization reversal dynamics in the media of magneto-optical recording," *J. Appl. Phys.*, **vol. 63**, pp. 5809-5823 (1988).